Desalination and Water Treatment
www.deswater.com

doi: 10.5004/dwt.2023.30181

316 (2023) 136–150
December

Comparative performance evaluation of two compression ways of a single-effect mechanical vapor compression desalination system

Cong Liu[a,b,*], Lin Xu[a,b], Yumeng Wang[a]

[a]*Shenyang Institute of Engineering, Shenyang, 110136, China, email: liucong@sie.edu.cn (C. Liu)*
[b]*Shenyang Institute of Engineering, Liaoning Engineering Technology Research Center for Biomass Energy Machinery and Equipment, Shenyang 110136, China*
[c]*Shenyang Institute of Engineering, Key Laboratory of Liaoning Province for Clean Combustion Power Generation and Heating Technology, Shenyang 110136, China*

Received 7 June 2023; Accepted 28 November 2023

ABSTRACT

The current study aims to conduct a comparative performance evaluation of two compression methods, namely high-temperature compression (HTC) and injected-water compression (IWC), within a single-effect mechanical vapor compression desalination system. The system performance of two compression methods is evaluated by establishing a thermodynamic model, exergy-analysis model, and thermo-economic model. The results indicate that, under identical input parameter conditions, the HTC system exhibits a 6% increase in freshwater production compared to the IWC system. However, the performance of the HTC system is inferior to that of the IWC system in other aspects, including nearly three times higher compression power consumption, a 40% reduction in the second law efficiency of the system, and a 30% increase in the simplified cost of water (SCOW). The impact of various design parameters, including the temperature and mass flow rate of the feedwater, as well as the vapor temperature and the temperature difference between saturated heating steam and vapor, on system performance is subsequently discussed. The investigation reveals that a lower feedwater temperature is associated with an increased recovery ratio, enhanced second law efficiency, and reduced SCOW. The feedwater mass flow rate does not impact distillate efficiency and energy efficiency but solely influences distillate production and the SCOW. The higher vapor temperature is advantageous as it enhances the recovery ratio and second law efficiency while reducing the SCOW. It is crucial to define a compromise value for the temperature difference between saturated heating steam and vapor. A high-temperature difference results in an increased SCOW, whereas a low-temperature difference restricts the feedwater temperature range.

Keywords: Comparative performance evaluation; Single-effect mechanical vapor compression desalination system; High-temperature compression; Injected-water compress

1. Introduction

Seawater desalination is considered a viable solution to overcome the freshwater scarcity problem [1]. There are three primary desalination technologies: membrane, adsorption technology, and evaporation processes. Membrane technology such as reverse osmosis (RO) is characterized by low energy consumption but has several disadvantages including high operation costs, strict requirements, and short membrane lifespan [2]. Recently, adsorption technology has been invested in desalination applications. In this technology, an adsorbent material with a high affinity to water like silica gel can be used to separate the water from the salts [3,4]. However, the adsorption technology has not been greatly developed and widely used. Thermal desalination

* Corresponding author.

technology can be involved in several categories such as multi-stage flash (MSF), multi-effect evaporation (MEE), thermal vapor compression, and mechanical vapor compression (MVC) [5]. The advantages associated with MVC systems are high-quality water recovery that needs little or no treatment, compact equipment, low operating cost, stable operation, and simple integration with renewable energy systems. MVC is known to be an attractive and competitive solution for medium-scale water reclamation desalination for production capacities of less than 5,000 m^3/d [6].

The concept of the MVC was initially introduced in 1969. Over several decades, it made great progress in theoretical and experimental research. Theoretical investigations primarily focus on elucidating the impact of different parameters and configurations on system performance through the establishment of various rigorous mathematical models. Al-Juwayhel et al. [7] conducted a comparative analysis of four different types of single-effect evaporator desalination systems and proposed a mathematical model to assess the performance ratio, specific power consumption, specific heat transfer area, and specific cooling water flow rate. In the MVC system, it was observed that the specific power consumption decreased as the boiling temperature increased and as its difference with the compressed vapor temperature widened. Ettouney et al. [8] analyzed the characteristics of single-effect MVC as a function of the system design and operating parameters. The results indicated that higher top brine temperatures and reduced temperature differences between boiling brine and steam condensate led to a decrease in specific power consumption. El-Dessouky et al. [9] presented a performance analysis for the vapor compression parallel feed multiple-effect evaporation water desalination system. The results demonstrated that, in the case of the parallel flow configuration, an increase in operating temperature led to a decrease in the conversion ratio. Aybar [10] investigated the operation characteristics of a low-temperature MVC desalination system. Ettouney [11] proposed a comprehensive design model of the single-effect mechanical vapor compression process with several new design features including the evaporator dimensions, demister dimensions, dimensions of the non-condensable gases venting orifice, and capacity of the vacuum system. Nafey et al. [12] developed exergy and thermal economic mathematical models for a multi-effect evaporation-mechanical vapor compression desalination process. The thermal performance ratio of the system, the unit product cost, the capital cost of the compressor, and specific power consumption are analyzed with/without external steam. Lara et al. [13] presented the detailed engineering and economics of an MVC system operating at 172°C. The utilization of elevated operating temperatures offers several advantages, including reduced compression work, minimized latent heat transfer area, and a compact compressor. Alasfour and Abdulrahim [14] proposed a hybrid MSF-MVC desalination system and studied the thermal performance of the MVC desalination system. Onishi et al. [15] introduced a new optimization model for the single and multiple-effect evaporation systems for shale gas flowback water desalination. The results highlighted the potential of the proposed model to cost-effectively optimize SEE/MEE systems by producing freshwater and reducing brine discharges and associated environmental impacts. Jamil and Zubair [16] focused on thermoeconomic analysis of a single-effect MVC desalination system operating with and without brine recirculation. Schwantes et al. [17] presented a technological design and economic analysis for membrane distillation and MVC for the same application. Elsayed et al. [18] studied exergy analysis of four different feed configurations of a multi-effect desalination with MVC system and proposed an exergy-economic model to assess the performance of a multi-effect desalination plant integrated into a mechanical vapor compressor unit (MED-MVC) [2].

Theoretical research is advancing rapidly, while simultaneously witnessing the construction of various experimental devices and commercial applications. Matz and Fisher [19] showed that MVC systems have an equal total production cost compared with the RO method. Lucas and Tabourier [20] introduced a 1,500 m^3/d unit constructed by Sidem installed in the Nuclear Power Plant of Flamanville in France. In 1994, more than 200 units with very small capacity were reported by Matz and Zimerman [21]. Veza [22] presented that the Las Palmas Port Authority desalination plant consists of two low-temperature vapor compression units with a production capacity of 500 m^3/d each. Kronenberg and Lokiec [23] described the practical commercial application for steam-driven multi-effect distillation plants in dual-purpose applications and the latest developments for single-purpose mechanical vapor compression plants. Wu et al. [24] presented a new single-effect MVC system with a rotating disk evaporator. Shen et al. [25] developed and applied a 50 m^3/d double-effect MVC system with a water-injected twin-screw compressor. Hong et al. [26] described the mathematical and experimental study of the MVC system driven by the roots compressor.

The vapor compressor is a critical component in the MVC system, significantly impacting its performance. It compresses the secondary steam generated in the evaporator to enhance its internal energy, which is then reused as input energy for the system. In previous literature, it was common to compress secondary vapor into superheated steam at high temperatures and pressure. However, with recent advancements in compressor technology, a water-injected compression technique has been developed and increasingly adopted. This technique involves injecting liquid water into the working chamber to lower the steam temperature at the compressor outlet [27]. When designing an MVC system, the designer's priority lies in determining the optimal compression method. However, there is a dearth of literature comparing the performance of different compression methods in MVC desalination systems. This paper presents a comprehensive evaluation of the thermodynamics, economics, and exergy analysis for two compression methods employed in a single-effect mechanical compression system. Additionally, mathematical models have been enhanced to incorporate critical factors such as the relationship between inlet/outlet temperatures of the preheater and distillate water, as well as the mass fraction of feedwater between two preheaters. The model results elucidate distinct characteristics of both compression methods theoretically and provide decision-makers with a foundation for selecting appropriate design approaches.

2. MVC system description

Fig. 1 depicts the schematic of a single-effect MVC process featuring two distinct compression methods, comprising a horizontal-tube falling film evaporator, two shell-tube-type preheaters, a vapor mechanical compressor, transfer pumps, and other components. The vacuum system is omitted for simplicity. The evaporator is a conventional horizontal-tube falling film evaporator including spray nozzles, vapor suction tube, horizontal heat-exchange tubes, and a wire mesh mist eliminator [28]. The preheater is selected as a shell-tube type because of its relatively simple manufacturing and adaptability to different operating conditions [29]. Currently, centrifugal, roots and screw compressors are the three main kinds of vapor compressors. Due to the advantage of good stability, larger compression ratio, and wet compression, a screw compressor is chosen as the main type for medium-scale water reclamation desalination [30].

Within the MVC system, seawater is directed to the preheaters for heat exchange with the distillate. The warmed brine then enters the evaporator and descends through a horizontal tube via a spray nozzle. A portion of the brine undergoes evaporation, generating secondary steam which is subsequently compressed by a vapor mechanical compressor to enhance its internal energy as input for the system. The main distinction between Fig. 1a and b lies in the compression process. In Fig. 1a the secondary steam undergoes compression from saturated to superheated state, whereas in Fig. 1b the secondary steam, mixed with a minimal amount of distillate water, is compressed to saturated steam at a lower temperature.

3. System modeling

Several mathematical models, including the thermodynamic, exergy-analysis, and thermo-economic models, have been developed to analyze the performance of a single-effect mechanical compression system with different compression methods and to investigate the effects of major design parameters.

The MVC system, being a complex and nonlinear system, necessitates the consideration of certain reasonable assumptions:

- Steady-state operation;
- Thermodynamic losses have been assumed to be 1°C as a real design value between the brine and the vapor in one evaporator [31];
- Steam is completed condensed at the end of the horizontal tubes;
- Compression process is assumed to be isentropic compression.

3.1. Thermodynamic model

A thermodynamic model is used to calculate the design parameters of the system and each node. The thermodynamic model mainly includes mass balance, energy balance, and salinity balance equations in the evaporator, compressor, and preheaters.

3.1.1. Evaporator model

Mass balance:

$$M_f = M_v + M_b \tag{1}$$

Energy balance:
High-temperature compression (HTC) system:

$$Q_e = \left(H_{s0} - H_s\right)M_s = M_v\lambda_{T_b} + M_f C_p\left(T_b - T_f\right) \tag{2}$$

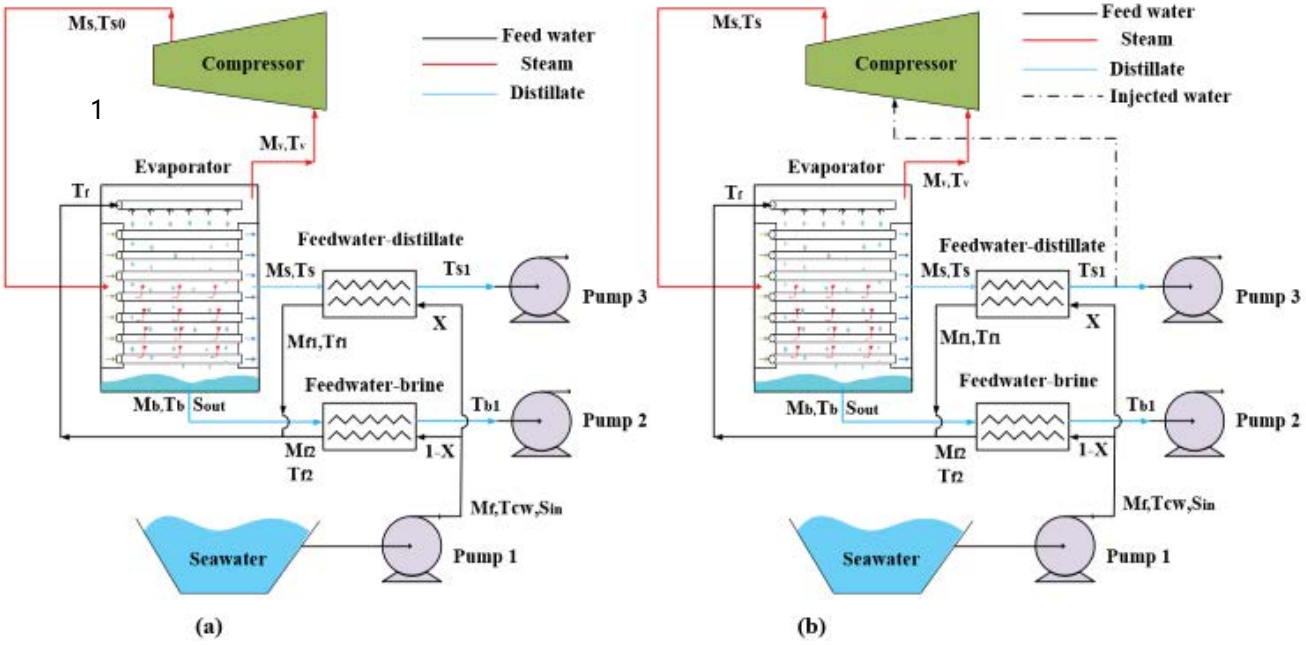

Fig. 1. Schematic of a single-effect MVC process with two different compression ways. (a) High-temperature compression and (b) injected-water compression.

Injected-water compression (IWC) system:

$$Q_e = M_s\lambda_s = M_v\lambda_{T_b} + M_f C_p\left(T_b - T_f\right) \tag{3}$$

Salinity balance:

$$M_f S_{\text{in}} = M_b S_{\text{out}} \tag{4}$$

where Q_e is the heat consumption in the evaporator, can be calculated as:

$$Q_e = h_e A_e \text{LMTD}_e \tag{5}$$

where A_e is the heat transfer area, h_e is the overall heat transfer coefficient, and for the sake of comparison it can be estimated according to Eq. (6) [32]:

$$h_e = 1961.9 + 12.6T_b - 9.6\times10^{-2}T_b^2 + 3.16\times10^{-4}T_b^3 \tag{6}$$

The logarithmic mean temperature difference LMTD_e is calculated:

HTC system:

$$\text{LTMD}_e = \frac{\left(T_{s0} - T_s\right) - \left(T_b - T_f\right)}{\ln\left(\dfrac{T_{s0} - T_s}{T_b - T_f}\right)} \tag{7}$$

IWC system

$$\text{LTMD}_e = \frac{T_b - T_f}{\ln\left(\dfrac{T_s - T_f}{T_b - T_f}\right)} \tag{8}$$

In one evaporator, the temperature difference between the brine temperature and the vapor temperature exists, which can be obtained by the following:

$$T_v = T_b - \left(\text{BPE} + \Delta T_h\right) \tag{9}$$

where BPE is the boiling point elevation, ΔT_h is the hydrostatic head loss [33], the sum of them is assumed to be 1°C.

3.1.2. Preheater model

The preheater model is based on energy balance and heat transfer equations. For simplified the design process, some assumptions are proposed:

- The counter current mode is used in the preheaters, that is heat flow and cold flow have opposite directions.
- The outlet temperature difference on both sides of the preheater is equal.

Taking feedwater-distillate preheater for example (Fig. 2), the energy that the distillate released equals that of the feedwater absorbs, which can be calculated:

$$Q_{p,1} = \text{Cp}_{s,T_s}\left(T_s - T_{s1}\right)M_s = \text{Cp}_{f,T_1}\left(T_{f1} - T_{\text{cw}}\right)M_{f1} \tag{10}$$

where M_s is the steam mass flow at the compressor outlet, M_{f1} is the seawater mass flow entering the feedwater-distillate preheater, it can be expressed by:

$$M_{f1} = M_f X \tag{11}$$

where X is the feed split between preheaters Eq. (10) is transformed:

$$\frac{M_{f1}}{M_s} = \frac{\text{Cp}_{s,T_s}}{\text{Cp}_{f,T_1}} = \frac{M_f X}{M_s} \tag{12}$$

where M_s/M_f = RR, the recovery ratio (RR) is an important parameter to measure the distillate efficiency of an MVC system.

Therefore, as shown in Eq. (13),

$$X = \frac{\text{Cp}_{s,T_s}}{\text{Cp}_{f,T_1}}\text{RR} \tag{13}$$

The feed split between preheaters X is not defined arbitrarily, it should be determined by various recovery ratios of an MVC system.

The heat exchange area can be calculated as follows:

$$Q_{p,1} = h_p A_{p,1}\text{LMTD}_{p,1} \tag{14}$$

where $\text{LMTD}_{p,1}$ is the logarithmic mean temperature difference, is determined by the following equation:

$$\text{LMTD}_{p,1} = \frac{\left(T_s - T_{f1}\right) - \left(T_{s1} - T_{\text{cw}}\right)}{\ln\left(\dfrac{T_s - T_{f1}}{T_{s1} - T_{\text{cw}}}\right)} \tag{15}$$

The overall heat transfer coefficients of the two preheaters are estimated according to Eq. (16):

$$h_p = 1.7194 + 3.2063\times10^{-3}T_v + 1.5971\times10^{-5}T_v^2 - 1.9918\times10^{-7}T_v^3 \tag{16}$$

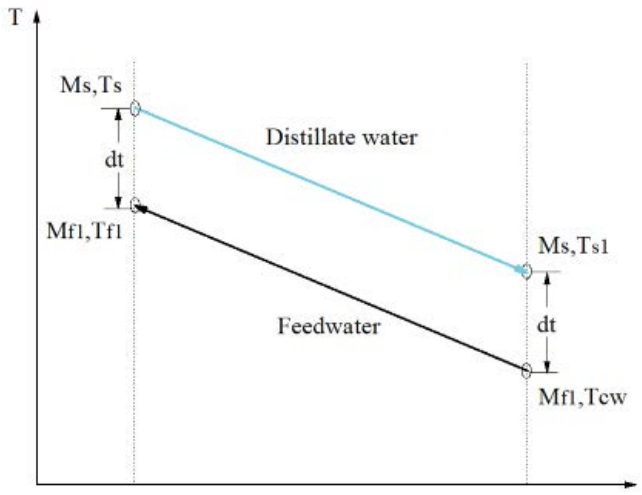

Fig. 2. Feedwater-distillate preheater temperature curve.

Similar to the feedwater-distillate preheater, the parameters of the feedwater-brine preheater are calculated:

$$Q_{p,2} = \mathrm{Cp}_{b,T_b}\left(T_b - T_{b1}\right)M_b = \mathrm{Cp}_{f,T_{\mathrm{cw}}}\left(T_{f2} - T_{\mathrm{cw}}\right)M_{f2} = h_p A_{p,2}\mathrm{LMTD}_{p,2} \tag{17}$$

$$M_{f2} = M_f - M_{f1} \tag{18}$$

$$\mathrm{LMTD}_{p,2} = \frac{\left(T_b - T_{f2}\right) - \left(T_{b1} - T_{\mathrm{cw}}\right)}{\ln\left(\frac{T_b - T_{f2}}{T_{b1} - T_{\mathrm{cw}}}\right)} \tag{19}$$

Leaving the preheaters, the temperature of two strands of the seawater increases and then join together. The mixing temperature is given as:

$$T_f = XT_{f1} + \left(1 - X\right)T_{f2} \tag{20}$$

3.1.3. Compressor model

For the sake of clear expression, two different compression ways high-temperature compression and injected-water compression are plotted in the T-S diagram (Fig. 3).

For the high-temperature compression process, point 2 represents the secondary steam in a saturated state, which is subsequently compressed to a superheated state within the compressor. The vertical lines 2-3 depict an isentropic compression process. Line 3-4-5 illustrates the condensation process where the superheated steam undergoes complete condensation within the tube. According to the energy balance, the compressor power can be calculated as follows:

$$W_c = M_v\left(H_3 - H_2\right) \tag{21}$$

where the subscript 2 and 3 denoted the point in the T-S diagram in Fig. 3.

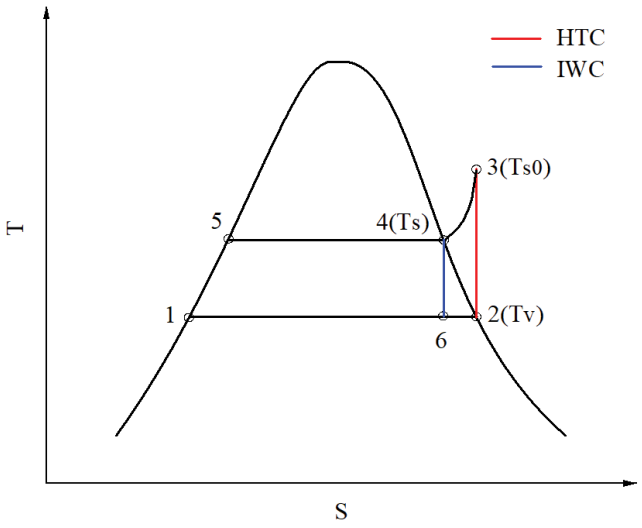

Fig. 3. Two different compression ways in a T-S diagram.

The calculation relation of temperature and pressure is determined by:

$$T_{s0} = T_v \cdot \left(\alpha\right)^{(\gamma-1)/\gamma} = T_v \cdot \left(\frac{P_{s0}}{P_v}\right)^{(\gamma-1)/\gamma} \tag{22}$$

where α is the pressure ratio, γ is the isentropic coefficient that is estimated to be 1.3 [11].

For the injected-water compression process, it is the heat transfer and phase change process of the same material [34]. The distillate water is introduced into the compressor to blend with the saturated vapor, effectively reducing the temperature of superheated steam at the outlet of the compressor. The mass fraction of injected-water in the compressor outlet total flow (x) is calculated by the following equation [13]:

$$x = \frac{S_2 - S_4}{S_4 - S_1} \tag{23}$$

The compressor power is determined based on the energy balance as:

$$W_c = M_s H_4 - M_v H_1 - xM_s H_2 \tag{24}$$

where S and H are entropy and enthalpy, respectively, the subscript of that are the point in the T-S diagram in Fig. 3.

The fluid flow into the compressor is the sum of the secondary steam and a small fraction of the condensed water, so:

$$M_s = M_v + xM_s \tag{25}$$

3.2. Exergy-analysis model

According to the second law of thermodynamics, in a natural process, under the condition without external energy input, the chaos ('entropy') of an isolated system does not increase. Second law efficiency is a key indicator to quantify how close the practical systems are to the thermodynamic limit. In general, second law efficiency is defined as the exergy change of the system to exergy input:

$$\eta_{\mathrm{II}} = \frac{\text{exergy change of the system}}{\text{exergy input}} = \frac{\Delta E}{W_t} \tag{26}$$

To sustain the operation of a mechanical vapor compression desalination system, additional external energy input such as a compressor and transfer pump is required. The exergy input to the system is the sum of the compressor and transfer pump power, which can be obtained:

$$W_t = W_c + \sum W_p \tag{27}$$

where W_c and W_p are the compressor power and transfer pump power, respectively.

The exergy change of the system is determined by the net exergy transfer across its boundaries. The specific exergy of a fluid stream with negligible kinetic and

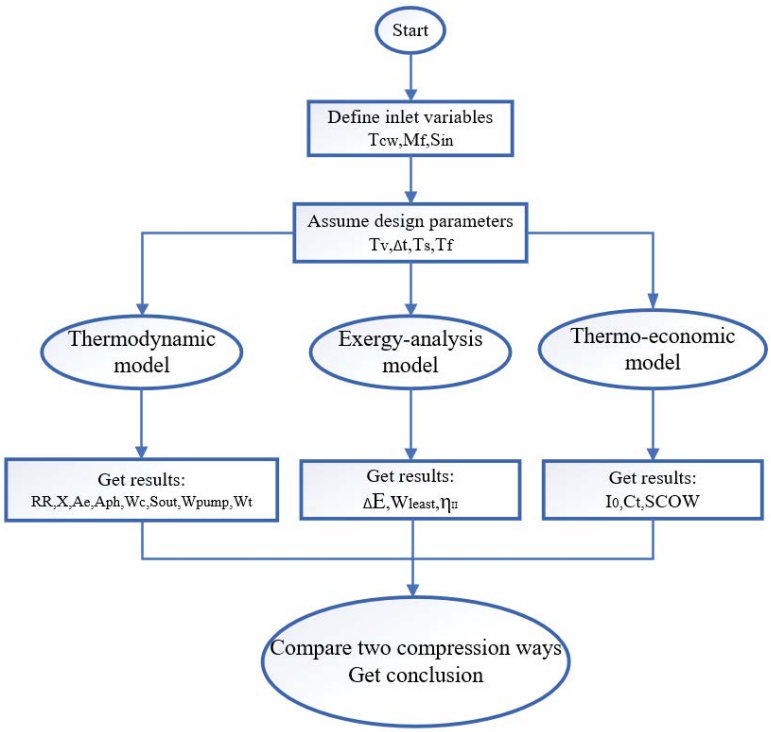

Fig. 4. Computational process of an MVC system.

potential energies is given by $e = h–h_0(s–s_0)$ [12]. So, the exergy change of the system can be calculated as:

$$\begin{aligned}\Delta E = {} & M_b\left[h_b - h_{0,b} - T_0\left(s_b - s_{0,b}\right)\right] \\ & + M_s\left[h_s - h_{0,s} - T_0\left(s_s - s_{0,s}\right)\right] \\ & - M_f\left[h_f - h_{0,f} - T_0\left(s_f - s_{0,f}\right)\right]\end{aligned} \tag{28}$$

3.3. Thermo-economic model

The thermo-economic model is primarily utilized for estimating the cost of the final product, which serves as a crucial criterion for comparing the commercial costs associated with two distinct compression methods.

In most papers [35], a parameter named the simplified cost of water (SCOW) is used to define the initial capital cost, which is given as:

$$\mathrm{SCOW} = \frac{\left(I_0 \cdot \varphi\right) + C_t}{M_s} \tag{29}$$

where the amortization factor (ϕ) is defined as:

$$\varphi = \frac{i\left(1+i\right)^n}{\left(1+i\right)^n - 1} \tag{30}$$

where i is the interest rate and n is the number of years of the economic life of the system, taken as 0.05 and 20, respectively [35]

In Eq. (30) it is assumed that every year (from year 1 to year n) the desalination plant produces the same amount of water (M_s) and has the same running cost (C_t).

Capital cost (I_0) refers to the total cost of the equipment at the initial investment that consists of hardware, engineering, construction, project management, initial design, permitting, and land etc. [36]. For the sake of comparison, the equipment and materials costs are only taken into account which is listed in Table 1.

Running cost (C_t) is the annual operating cost which mainly includes the cost of energy (heat and electricity), seawater pretreatment chemicals, labor, maintenance, and management, which are listed in Table 2.

4. Computational method and process

The present study develops a set of computational procedures in Python language for the design and calculation of the MVC system. An additional advantage of utilizing Python is its convenience in calculating the physical properties of water vapor and brine, facilitated by an IAPWS module.

In the computational process, inlet variables are first defined including seawater temperature T_{cw}, seawater mass flow rate M_f, and seawater salinity S_{in}. Then the secondary steam temperature T_v, the temperature difference between the heating steam and the secondary steam Δt, and the feedwater temperature are assumed. The above variables and parameters are input into the three mathematical models to calculate the rest of the detailed results. Finally, the paper concludes by comparing two compression methods. The required input parameters used for the MVC system simulation are defined in Table 3.

Table 1
Main compositions of the capital cost

Component	Symbol	Equation	Description	References
Evaporator	Z_{evap}	$Z_{evap} = C\cdot(A_e)^{\gamma}$	C = 300 \$/m^2, γ = 0.95	[37]
Preheater	Z_{pre}	Z_{pre} = 1,000(12.86 + $A_p^{0.8}$)	None	[38]
Compressor	Z_{comp}	$Z_{comp} = 7{,}364 m_v\cdot\alpha\cdot e^{0.7}$	$10 \le m_v \le 455$, $1.1 \le \alpha \le 2$, $2.3 \le e \le 11.5$, $e = \frac{\eta_{comp}}{1-\eta_{comp}}$	[39]
Pump	Z_{pump}	$Z_{pump} = 13.92 m_{water}\Delta p^{0.55} e^{1.05}$	$2 \le m_{water} \le 32$, $100 \le \Delta p \le 6{,}200$, $1.8 \le e \le 9$, $e = \frac{\eta_{pump}}{1-\eta_{pump}}$	[16]
$I_0 = Z_{evap} + Z_{pre} + Z_{comp} + Z_{pump}$				

Table 2
Main compositions of the running cost

Parameters	Symbol	Equation	Description	References
Electricity	C_{el}	$C_{el} = 365\times 24\times P_{el}\times W_{pump}\times M_{sw}$	P_{el} is unit electricity price 0.07 \$/kWh, W_{pump} is the sum of pump power consumption in kWh/m^3	[40]
Seawater pretreatment	C_{sp}	$C_{sp} = M_{ft} m_{cc} P_c$	m_{cc} is chemical consumption per ton seawater 0.005 kg/ton, P_c is the unit chemical cost 1.46 \$/kg	[40]
Operators' salary	C_{os}	$C_{os} = 6000\times 6$	The yearly operators' salary is 6,000\$/operator with the plant using 6 operating workers	[40]
Maintenance cost	C_{mt}	$C_{mt} = 1.5\%\times I_0$	The annual maintenance cost is estimated as 1.5% of the capital cost	[40]
Management cost	C_{mg}	$C_{mg} = 20\%\times C_{os}$	The annual management cost is estimated as 20% of the labor cost	[40]
$C_t = C_{el} + C_{sp} + C_{os} + C_{mt} + C_{mg}$				

Table 3
Required input parameters

Feedwater mass flow rate, kg/s	M_f	10~60
Seawater temperature, °C	T_{cw}	28 [41]
Seawater salinity, g/kg	S_{in}	45.0 [42]
Maximum allowable brine salinity, g/kg	S_{out}	60.0~160.0
Secondary steam temperature, °C	T_v	40~90
Temperature difference between the heating steam and the secondary steam, °C	Δt	5~25 [27]
Thermal efficiency of the compressor	η_{comp}	0.85
Thermal efficiency of the pump	η_{pump}	0.85

5. Results and discussion

5.1. Model accuracy verification

For substantiation of the accuracy of the mathematic models of two compression ways of the MVC system, the model results from Jamil and Zubair [16] and calculated by the mathematic models in the paper are compared in Table 4.

As shown in Table 4, the HTC model results fit well with that of Jamil and Zubair [16] with a minor error below 3%. With the same high-temperature compression way the HTC model and the Jamil and Zubair [16] lead to minor differences. This shows that the HTC model in the paper is reliable.

As the IWC model has been proposed in recent years, few experimental data on the IWC model in an MVC system appeared in the previous literature. Although the IWC model has not been verified by the experimental data, the injected-water compressor theory in the paper has been introduced in many references. This work is mainly focused on the performance comparison of the two models at the numerical simulation. The results indicate that under the same parameter conditions, the compressed vapor temperature of the HTC model is higher and exhibits a larger recovery

ratio and plant capacity compared to the IWC mathematical model (Table 4). Furthermore, additional distinctions between these two models.

The same input parameters are essential for comparing the performance of the two systems. Under the same parameter input condition of M_f = 10 kg/s, T_v = 60°C, T_f = 57°C, Δt = 10°C, the detailed results of the two systems are listed in Table 5.

The primary distinction between the two systems lies in their compression methods, as illustrated in Table 5. Under identical temperature differentials between the heating steam and secondary steam, along with a constant compression ratio, the HTC system exhibits significantly higher steam temperatures at the compressor outlet compared to the IWC system. Consequently, this results in a nearly threefold increase in compression power for the former when compared to the latter.

Due to the higher enthalpy of superheated steam entering the evaporator in the HTC system compared to saturated steam in the IWC system, a larger amount of heat

Table 4
Comparison based on the study of Jamil & Zubair [16] and model results

Parameters	Jamil and Zubair [16]	HTC model	IWC model
Intake seawater temperature, °C	21	21	21
Feed seawater temperature, °C	61	61.6	61.6
Evaporation temperature, °C	63	63	63
Vapor temperature, °C	61.9	62	62
Compressed vapor temperature, °C	81	80.7	67
Compression ratio, α	1.29	1.25	1.25
Intake seawater salinity, g/kg	40	40	40
Brine salinity, g/kg	80	82	65
Feed split ratio between preheaters, X, %	50	50	50
Feed flow rate, kg/s	26	26	26
Plant capacity, kg/s	13	13.52	9.88
Recovery ratio, RR	0.5	0.52	0.38

Table 5
Detailed comparison results of the two systems

	Thermodynamic model				
	HTC system	IWC system		HTC system	IWC system
T_{s0}, °C	98.2	–	Q_e, kW	13,990	12,778
T_s, °C	70	70	A_e, m^2	79.5	88
T_b, °C	61	61	$A_{p,1}$, m^2	13.3	12
T_{b1}, °C	46	46	$A_{p,2}$, m^2	7	10
T_{s1}, °C	30.6	31.2	M_s, kg/s	5.9	5.3
T_f, °C	57	57	M_b, kg/s	4.1	4.7
T_{f1}, °C	68.8	68.9	Recovery ratio	0.59	0.53
T_{f2}, °C	39.5	43	Feedwater split between preheaters, X	0.6	0.54
T_{cw}, °C	28	28	Compression ratio, α	1.56	1.56
W_{com}, kW	320	92			
	Exergy-analysis model				
	HTC system	IWC system		HTC system	IWC system
ΔE, kW	56	54	η_{II}	17.6%	59%
	Thermo-economic model				
	HTC system	IWC system		HTC system	IWC system
Z_{evap}, $	19,165	21,142	Z_{comp}, $	227,248	209,915
Z_{pre}, $	23,972	24,977	Z_{pump}, $	52,492	52,492
C_t, $	247,188	106,748	SCOW, $/ton	2.82	2.16
I_0, $	323,880	307,521			

power is released during condensation, resulting in a 9% reduction in required heat transfer area and a 6% increase in total freshwater production. When comparing the freshwater output performance of both systems under similar input parameters, it can be concluded that the HTC system outperforms the IWC system.

The exergy-analysis model is used to calculate the exergy loss and second-law efficiency of the system. The exergy loss remains nearly identical due to the negligible disparity in the inlet and outlet parameters between the two systems. However, there is a significant difference in the second law efficiency between the two systems, with values of 17.6% and 59%, respectively. This discrepancy can be attributed to the fact that the exergy input for compression power in the HTC system far exceeds that of the IWC system. As per Eq. (26), the denominator is inversely proportional to this ratio, meaning that a higher exergy input corresponds to lower second-law efficiency. In terms of energy efficiency, it can be concluded that the IWC system outperforms the HTC system.

The cost of the desalination plant serves as a crucial criterion for decision-makers, representing a significant indicator to assess the economic viability of a system model. According to the thermo-economic model analysis, the cost of both the evaporator and preheater is determined by the heat transfer area. Consequently, the evaporator cost in the HTC system exhibits a reduction of approximately 10% compared to that in the IWC system, while the cost difference for preheaters between these two systems remains below 4%. Given the relatively low sensitivity of compression power to compressor cost, the HTC system exhibits over three times higher power compared to the IWC system, with a mere 8% increase in cost. Overall, considering total capital costs, there is no significant disparity between the HTC and IWC systems.

However, the running cost of the HTC system is almost 2 times much more than that of the IWC system. That is because the electricity cost that is directly proportional to the compression power plays the most important part in running costs with 80% and 53%, respectively (Table 6). Although the total freshwater production of the HTC system is higher, the cost of the system increases more seriously, which leads to the simplified cost of water per mass flow of the HTC model is about 30% more than that of the IWC model.

As discussed above, at the same parameters input conditions, the HTC system has an advantage over the IWC system in terms of freshwater production about a 6% increase, while it is far inferior to the IWC system in other aspects, such as almost 3 times on compression power, 40% decrease on the second law efficiency of the system, 30% more on the simplified cost of water per mass flow. The aforementioned conclusions are derived from specific input parameters, and further discussion is required to explore the impact of variations in these parameters on system performance. Therefore, this detailed analysis focuses on four key parameters: compression power, recovery ratio, SCOW, and second law efficiency. These parameters exhibit significant disparities in the calculation results between the two models.

Table 6
Compositions of the running cost of two systems (a) HTC model and (b) IWC model

	HTC model	IWC model
Electricity	80%	53%
Labor	14%	34%
Management	3%	7%
Maintenance	2%	4%
Chemical	1%	2%

5.2. Determination and effect of the feedwater temperature

In conventional MEE system design, the feedwater temperature is typically assumed to be several degrees lower than the heating steam temperature. However, for the single-effect MVC system, the determination of feedwater temperature is not arbitrary and requires specific calculations within a defined range. The phenomenon is explained as follows:

Taking the HTC system as an example, according to Eq. (2), feedwater temperature can be expressed as:

$$T_f = T_b - \frac{\left(H_{s0} - H_s - \lambda_{T_b}\right)M_s + \left(M_s - M_v\right)\lambda_{T_b}}{M_f C_p} \tag{31}$$

The recovery ratio can be obtained by:

$$\mathrm{RR} = \frac{\left(T_b - T_f\right)C_p}{H_{s0} - H_s - \lambda_{T_b}} \tag{32}$$

For the MEE or multi-effect MVC system, $M_s > M_v$ satisfies the requirement. In the single-effect recirculation MVC system M_s must equal to M_v, which leads to a narrow range of the feedwater temperature than that of the MEE or multi-effect MVC system.

Under the other constant design conditions, feedwater temperature mainly affects the distillate production and Recovery ratio. At M_f = 10 kg/s, T_v = 60°C, Δt = 10°C, the feedwater temperature and the Recovery ratio are listed in Fig. 5.

The recovery ratio decreases with an increase in feedwater temperature, as observed in Fig. 5. This can be attributed to the gradual enlargement of the molecular size of Eq. (32) due to the rise in feedwater temperature and constant brine temperature. The HTC model exhibits a larger variation magnitude compared to the IWC model. Furthermore, at the same feedwater temperature, the HTC system demonstrates a higher recovery ratio than that of the IWC system. In the HTC system, superheated steam serves as the heat source, while saturated steam is utilized in the IWC system. Consequently, hotter steam results in increased production of secondary steam. In the paper, the maximum allowable brine salinity is defined from 60 to 160 g/kg corresponding with the recovery ratio from 0.32 to 0.73. The superposition part of the temperature range of the two compression models in Fig. 5 is considered to be the feedwater temperature simulation range.

In the feedwater temperature simulation range, the effect of the variation of the feedwater temperature will be discussed. With the feedwater temperature increase, the recovery ratio, compression power, and second law efficiency of the two models have a downward trend (Fig. 6a, b, and d). However, increasing the compression power does not lead to a simultaneous increase in the specific cooling water consumption (SCOW) affected by distillate production. The SCOW has been observed to increase with an increase in feedwater temperature (Fig. 6c). Considering all factors comprehensively within the simulation range, it is more appropriate to maintain a lower temperature despite the larger compression power resulting in a higher recovery ratio, second-law efficiency, and lower SCOW.

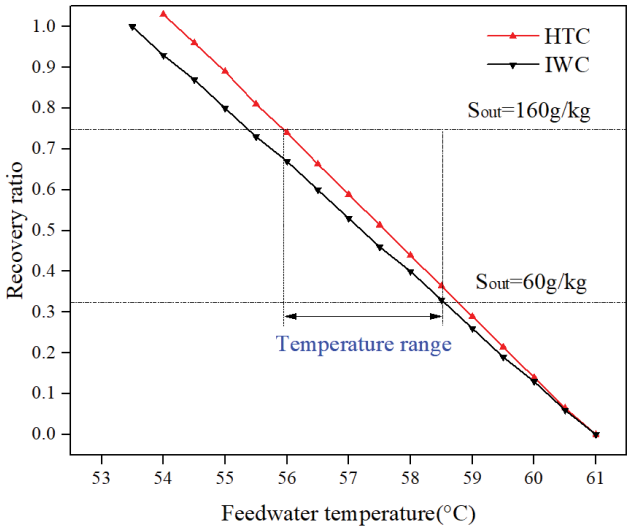

Fig. 5. Recovery ratio with feed temperatures.

5.3. Effect of the feedwater mass flow rate

The feedwater mass flow rate is a crucial parameter for determining the system's capacity and processing capability. Under the special parameters T_f = 57°C, T_v = 60°C, Δt = 10°C, with the increase of the feedwater mass flow rate (from 10 to 60 kg/s) the compression power has a linear increase (Fig. 7). The higher the feedwater mass flow rate, the larger the disparity between HTC and IWC models. At other constant parameters, the recovery ratio and second law efficiency remain constant. These results show that feed seawater flow rate only affects plant capacity, not distillate efficiency. The reason for this is that, by Eq. (32), the recovery ratio remains unaffected by variations in the feedwater mass flow rate. In terms of freshwater cost, an increase in the feedwater mass flow rate leads to a decline in SCOW. Initially, the SCOW experiences a rapid decline, while at flow rates exceeding 25 kg/s, the SCOW undergoes significant changes. During the design phase, it may seem

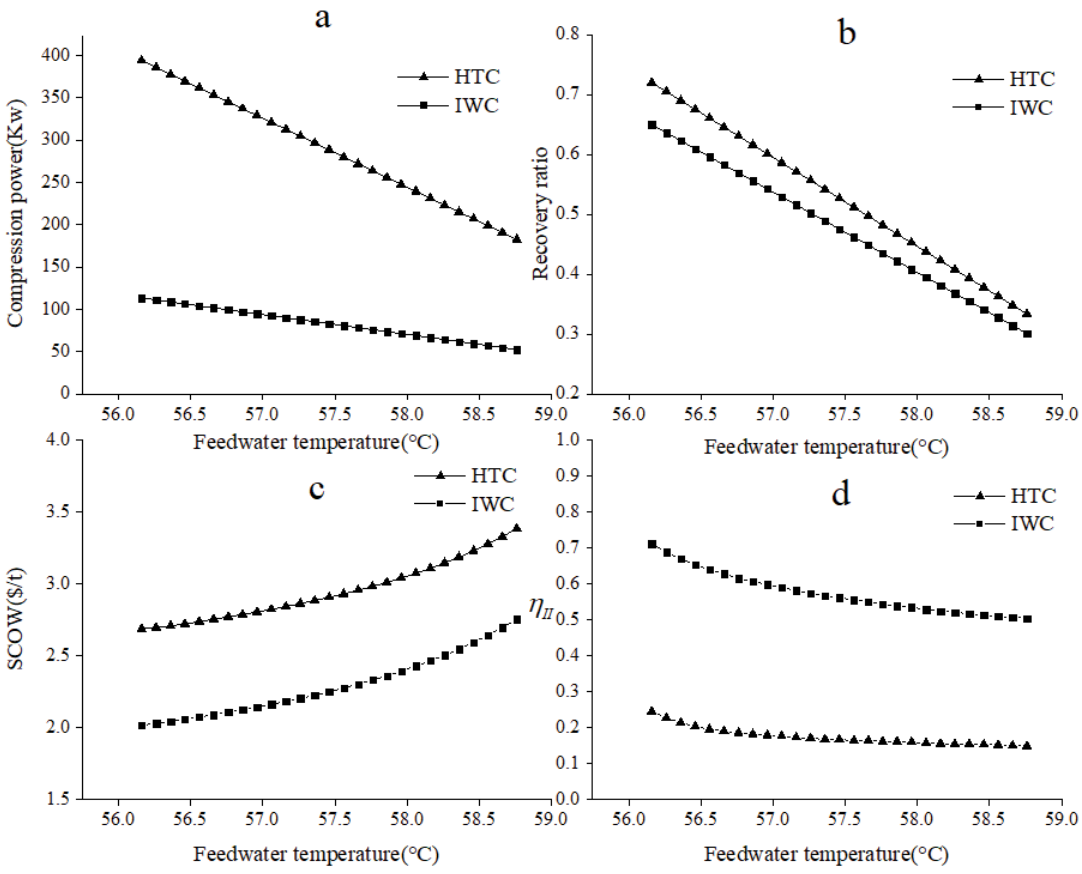

Fig. 6. Compression power (a), recovery ratio (b), SCOW (c), and η_{II} (d) with feedwater temperatures.

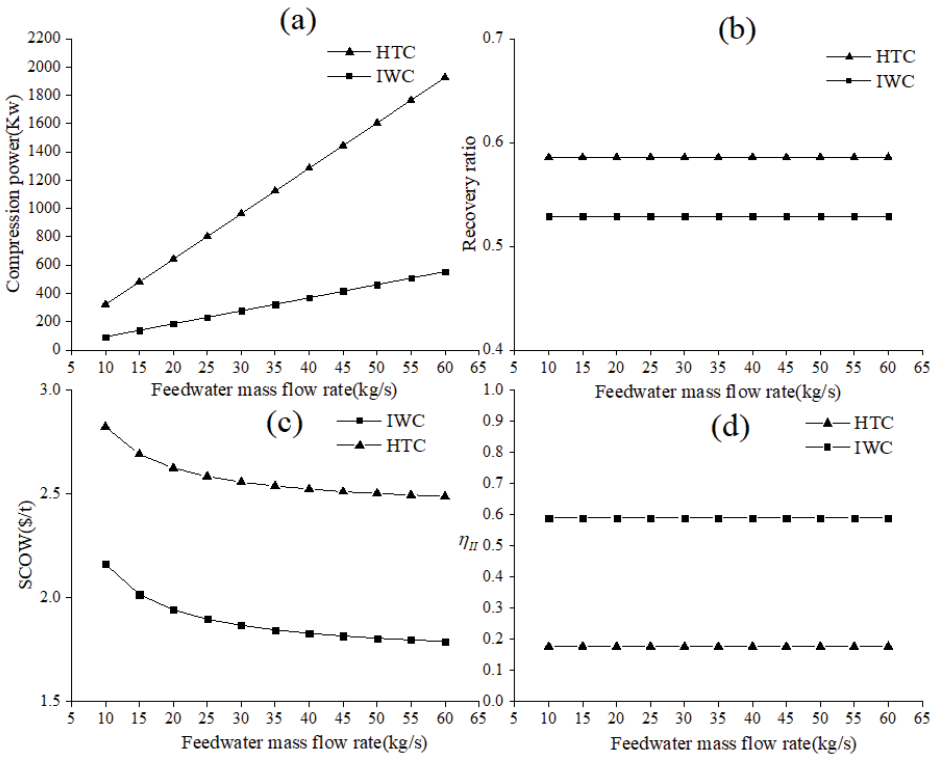

Fig. 7. Compression power (a), recovery ratio (b), SCOW (c), and η_{II} (d) with feedwater mass flow rate.

straightforward to opt for a higher feedwater mass flow rate to achieve increased distillate production and reduced freshwater costs. However, decision-makers must consider that higher capacity entails additional floor space requirements and manufacturing complexities.

5.4. Effect of the vapor temperature

At the condition of M_f = 10 kg/s, Δt = 10°C, $T_f = T_v$–2, the effect of the variations of the vapor temperature (between 40°C and 90°C) are discussed in this section. The vapor temperature corresponds to the compressor's inlet temperature, exerting a significant influence on the compression power. According to the operational principle of the compressor, an increase in the inlet vapor temperature leads to a heightened level of compression difficulty. With an increase in vapor temperature, the compression power exhibits an upward trend (Fig. 8a). Although the high vapor temperature corresponds to the bigger compression power, it leads to a bigger recovery ratio, second law efficiency, and lower SCOW which is beneficial for the MVC system. The higher vapor temperature should be better when designing the system. However, high vapor temperature will bring serious scaling problems. It is reasonable to define a high vapor temperature while avoiding scaling problems.

5.5. Effect of the temperature difference of the saturated heating steam and the vapor

Although the temperature difference between the saturated heating steam and the vapor remains consistent for both compression models, it corresponds to distinct compressor processes. For the IWC system, the temperature difference refers to the increase in temperature between the outlet and inlet points. In contrast, for the HTC system, it represents the temperature difference between the compressor inlet and saturated steam, rather than including superheated steam from the compressor outlet (Fig. 9). The increase in temperature difference primarily impacts the compression ratio, as illustrated in Fig. 10. This results in the upward movement of the apex of the isentropic line (from point 3 to point 3′). Under the parameters of T_v = 60°C, M_f = 10 kg/s, a curve of the compression ratio with the temperature difference is demonstrated in Fig. 10. With the increase in temperature difference, there is a linear upward trend observed in the compression ratio, leading to a simultaneous rise in compression power. However, it should be noted that while compression power is not the decisive indicator for evaluating system performance, further discussion will focus on exploring recovery ratio and SCOW as more significant parameters.

The recovery ratio from 0.32 to 0.73, as illustrated in Fig. 11, corresponds to different feedwater temperature ranges under various temperature differences. The increase in temperature difference leads to an expansion of the feedwater temperature range. The extended operational temperature range can effectively mitigate the impact of manufacturing errors on system performance. Another advantage of the significant temperature difference lies in its ability to induce variations in the Recovery ratio between the two models. At lower temperature differences (between 5 and 15), the HTC model exhibits a higher recovery ratio

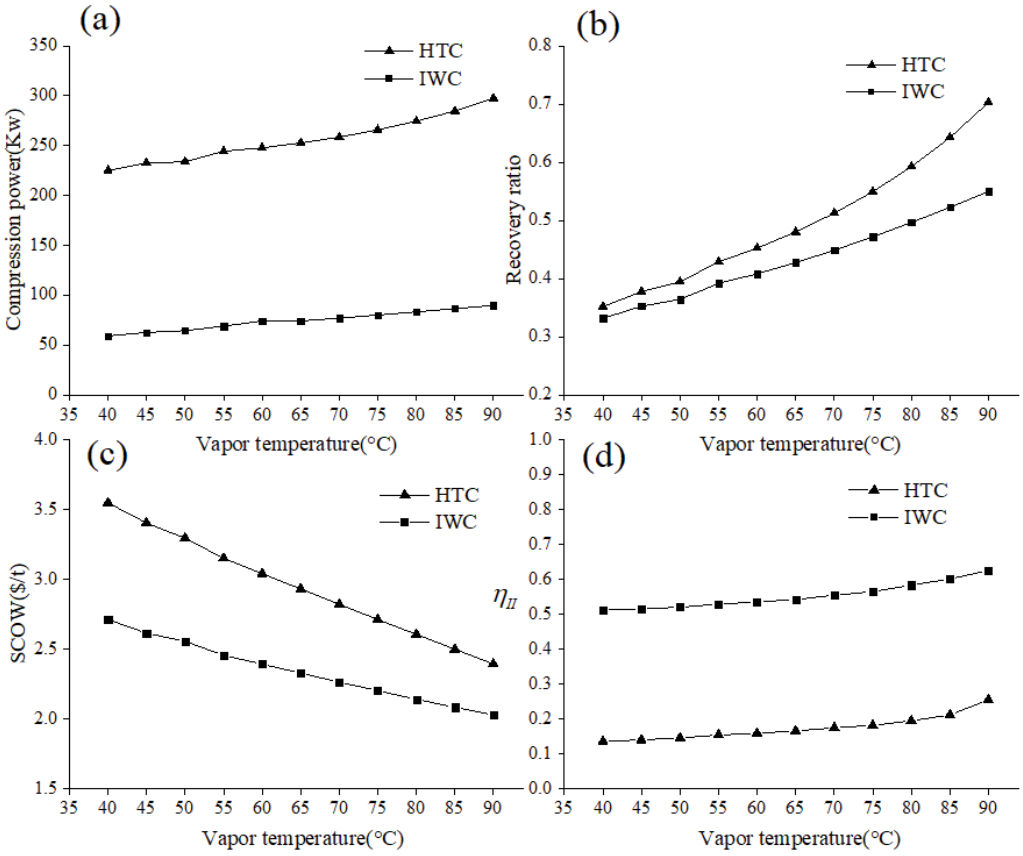

Fig. 8. Compression power (a), recovery ratio (b), SCOW (c), and η_{II} (d) with vapor temperature.

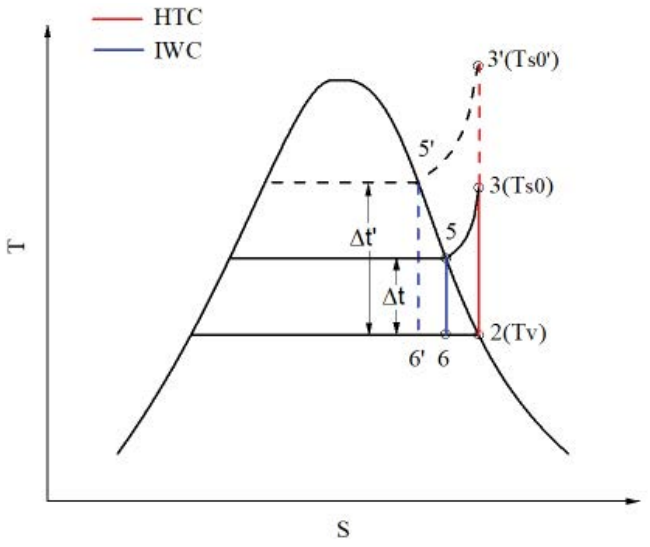

Fig. 9. Variation of the temperature difference in a T-S diagram.

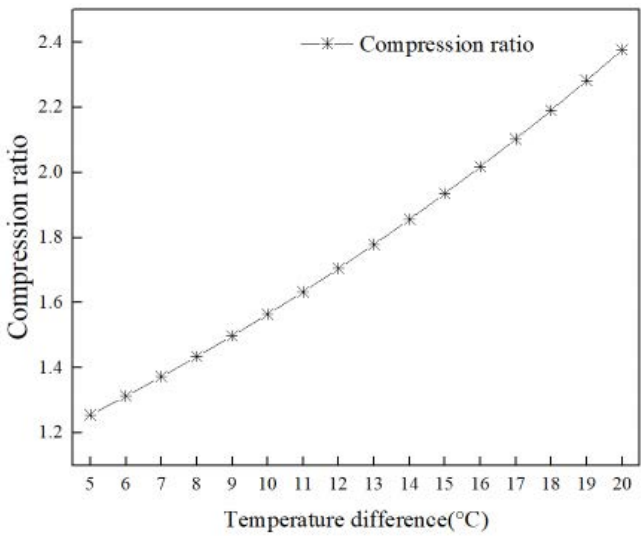

Fig. 10. Compression ratio with the temperature difference.

compared to the IWC system. As the temperature difference increases, the error in the recovery ratio diminishes. As discussed earlier, while having a superior recovery ratio is one of the HTC model's key advantages, it falls short when compared to the IWC model in various aspects. However, this advantage disappears at higher temperature differences. Therefore, when designing an MVC system under high-temperature differences with saturated heating steam and vapor conditions, choosing the IWC model undoubtedly becomes preferable.

In terms of the freshwater cost, a larger temperature difference leads to an increased SCOW (Fig. 12). While

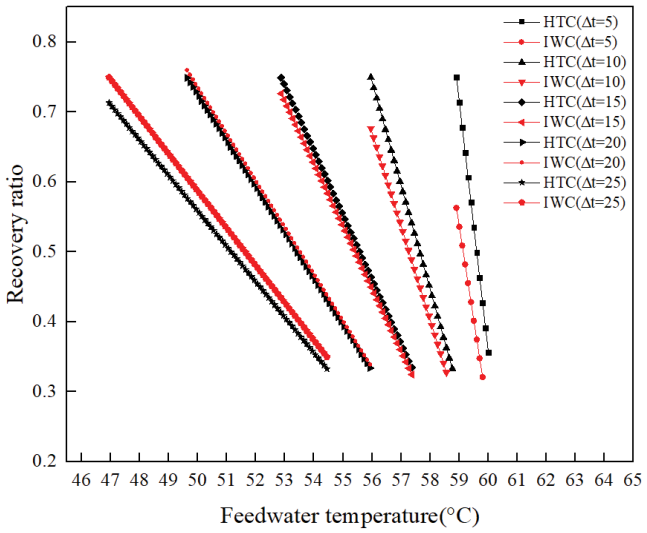

Fig. 11. Recovery ratio with the feedwater temperature under various temperature differences.

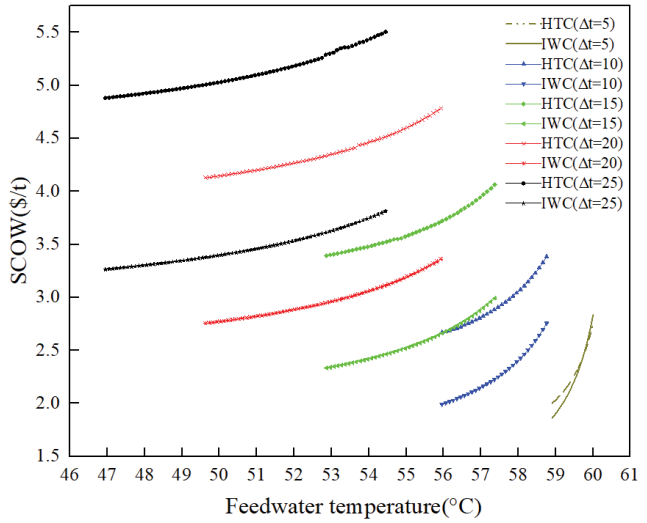

Fig. 12. SCOW with the feedwater temperature under various temperature differences.

theoretically, a smaller temperature difference may be preferable when designing an MVC system, it should be noted that a narrower feedwater temperature range associated with this choice is challenging to control in practical applications. This can result in minor errors having significant impacts on system performance. From my perspective, prioritizing stable operation states outweighs marginal freshwater savings. Therefore, defining a compromise temperature difference that offers a wider operating range and moderate SCOW is more favorable.

6. Conclusion

The paper introduces two distinct compression methods, namely high-temperature compression (HTC) and injected-water compression (IWC), for a single-effect MVC desalination system. Subsequently, thermodynamic modeling, exergy-analysis modeling, and thermo-economic modeling are established to facilitate the comparative performance evaluation of these two compression approaches.

The results indicate that, under identical input parameter conditions, the HTC model exhibits a 6% increase in freshwater production compared to the IWC model. However, it significantly lags behind the IWC model in other aspects: compression power is nearly three times higher, second law efficiency of the system experiences a 40% decrease, and there is a 30% higher simplified cost of water per mass flow.

The impact of various design parameters, including the feedwater temperature, feedwater mass flow rate, vapor temperature, and the temperature difference between the saturated heating steam and the vapor on system performance is discussed.

It has been observed that within the simulation range, a lower feedwater temperature is more suitable due to its higher Recovery ratio, second-law efficiency, and lower SCOW. The distillate efficiency and energy efficiency are not affected by the feedwater mass flow rate. This implies that as the feed seawater flow rate increases, the amount of distillate produced also increases while maintaining a constant recovery ratio and second-law efficiency. Although an increase in feedwater mass flow rate results in higher total freshwater cost, there is a decreasing trend in the simplified cost of water per mass flow. A higher vapor temperature yields greater benefits concerning recovery ratio, second law efficiency, and lower SCOW.

The significant temperature disparity between the saturated heating steam and vapor enables a broad operational range, capable of accommodating system fluctuations resulting from uncertain factors. However, this may lead to increased costs associated with freshwater consumption. Consequently, it is deemed impractical to define a high-temperature difference when designing an MVC system.

Symbols

M_f — Mass flow rate of feed water, kg/s
M_{f1} — Mass flow rate of feed water in Feedwater-distillate preheater, kg/s
M_{f2} — Mass flow rate of feed water in Feedwater-brine preheater, kg/s
M_s — Mass flow rate of heating steam, kg/s
M_b — Mass flow rate of brine, kg/s
M_v — Mass flow rate of vapor, kg/s
T_{cw} — The seawater temperature, °C
T_{f1} — Outlet feed water temperature of the Feedwater-distillate preheater, °C
T_{f2} — Outlet feed water temperature of the feedwater-brine preheater, °C
T_f — Feed water temperature, °C
T_b — Remaining brine temperature, °C
T_{s0} — Outlet vapor temperature of the compressor of the HTC system, °C
T_s — Outlet vapor temperature of the compressor of the IWC system, °C
T_v — Vapor temperature, °C
T_{s1} — Outlet water temperature of the feedwater-distillate preheater, °C

T_{b1} — Outlet water temperature of the feedwater-brine preheater, °C
X — Feed split between preheaters
H_{s0} — Enthalpy value of the outlet vapor of the compressor of HTC system, kJ/kg
H_s — Enthalpy value of the outlet vapor of the tubes of HTC system, kJ/kg
C_p — Specific heat at a constant pressure of seawater, kJ/kg·K
λ — Latent heat of evaporation, kJ/kg
S — Salt mass fraction, g/kg
A — Heat transfer area, m²
Q — Special heat consumption, kW
h — Heat transfer coefficient, W/m²·K
LMTD — Log mean temperature difference, °C
RR — Recovery ratio
BPE — Boiling point elevation, °C
dt — Temperature difference of the outlet hot flow and cold flow, °C
W_c — Power of the compressor, kW
P_{s0} — Outlet vapor pressure of the compressor, kPa
P_v — Inlet vapor pressure of the compressor, kPa

Subscripts

in — Parameters entering the effect
out — Parameters leaving the effect
s — Steam
b — Brine
e — Evaporator
f — Feed
v — Vapor
p — Preheater
1 — Feedwater-distillate preheater
2 — Feedwater-brine preheater

References

[1] D. Saldivia, C. Rosales, R. Barraza, L. Cornejo, Computational analysis for a multi-effect distillation (MED) plant driven by solar energy in Chile, Renewable Energy, 132 (2019) 206–220.
[2] M.L. Elsayed, O. Mesalhy, R.H. Mohammed, L.C. Chow, Transient and thermo-economic analysis of MED-MVC desalination system, Energy, 167 (2019) 283–296.
[3] K. Sztekler, W. Kalawa, W. Nowak, L. Mika, S. Gradziel, J. Krzywanski, E. Radomska, Experimental study of three-bed adsorption chiller with desalination function, Energies, 13 (2020) 1–13.
[4] P.G. Youssef, R.K. Al-Dadah, S.M. Mahmoud, Comparative analysis of desalination technologies, Energy Procedia, 61 (2014) 2604–2607.
[5] I.S. Al-Mutaz, I. Wazeer, Comparative performance evaluation of conventional multi-effect evaporation desalination processes, Appl. Therm. Eng., 73 (2014) 1192–11201.
[6] R. Borsani, S. Rebagliati, Fundamentals and costing of MSF desalination plants and comparison with other technologies, Desalination, 182 (2005) 29–37.
[7] F. Al-Juwayhel, H. El-Dessouky, H. Ettouney, Analysis of single-effect evaporator desalination systems combined with vapor compression heat pumps, Desalination, 114 (1997) 253–275.
[8] H. Ettouney, H. El-Dessouky, Y. Al-Roumi, Analysis of mechanical vapour compression desalination process, Int. J. Energy Res., 451 (1999) 431–451.
[9] H.T. El-Dessouky, H.M. Ettouney, F. Al-Juwayhel, Multiple effect evaporation-vapour compression desalination processes, Chem. Eng. Res. Des., 78 (2000) 662–676.
[10] H.S. Aybar, Analysis of a mechanical vapor compression desalination system, Desalination, 142 (2002) 181–186.
[11] H. Ettouney, Design of single-effect mechanical vapor compression, Desalination, 190 (2006) 1–15.
[12] A.S. Nafey, H.E.S. Fath, A.A. Mabrouk, Thermoeconomic design of a multi-effect evaporation mechanical vapor compression (MEE-MVC) desalination process, Desalination, 230 (2008) 1–15.
[13] J.R. Lara, G. Noyes, M.T. Holtzapple, An investigation of high operating temperatures in mechanical vapor-compression desalination, Desalination, 227 (2008) 217–232.
[14] F.N. Alasfour, H.K. Abdulrahim, The effect of stage temperature drop on MVC thermal performance, Desalination, 265 (2011) 213–221.
[15] V.C. Onishi, A. Carrero-Parreño, J.A. Reyes-Labarta, R. Ruiz-Femenia, R. Salcedo-Díaz, E.S. Fraga, J.A. Caballero, Shale gas flowback water desalination: single vs. multiple-effect evaporation with vapor recompression cycle and thermal integration, Desalination, 404 (2017) 230–248.
[16] M.A. Jamil, S.M. Zubair, On thermoeconomic analysis of a single-effect mechanical vapor compression desalination system, Desalination, 420 (2017) 292–307.
[17] R. Schwantes, K. Chavan, D. Winter, C. Felsmann, J. Pfafferott, Techno-economic comparison of membrane distillation and MVC in a zero liquid discharge application, Desalination, 428 (2018) 50–68.
[18] M.L. Elsayed, O. Mesalhy, R.H. Mohammed, L.C. Chow, Performance modeling of MED-MVC systems: exergy-economic analysis, Energy, 166 (2019) 552–568.
[19] R. Matz, U. Fisher, A comparison of the relative economics of sea water desalination by vapour compression and reverse osmosis for small to medium capacity plants, Desalination, 36 (1981) 137–151.
[20] M. Lucas, B. Tabourier, The mechanical vapour compression process applied to seawater desalination: a 1,500 ton/day unit installed in the nuclear power plant of Flamanville, France, Desalination, 52 (1985) 123–133.
[21] R. Matz, Z. Zimerman, Low-temperature vapour compression and multi-effect distillation of seawater. Effects of design on operation and economics, Desalination, 52 (1985) 201–216.
[22] J.M. Veza, Mechanical vapour compression desalination plants - a case study, Desalination, 101 (1995) 1–10.
[23] G. Kronenberg, F. Lokiec, Low-temperature distillation processes in single- and dual-purpose plants, Desalination, 136 (2001) 189–197.
[24] H. Wu, Y. Li, J. Chen, Research on an evaporator-condenser-separated mechanical vapor compression system, Desalination, 324 (2013) 65–71.
[25] J. Shen, Z. Xing, K. Zhang, Z. He, X. Wang, Development of a water-injected twin-screw compressor for mechanical vapor compression desalination systems, Appl. Therm. Eng., 95 (2016) 125–135.
[26] H. Hong, W. Li, C. Gu, Performance study on a mechanical vapor compression evaporation system driven by roots compressor, Int. J. Heat Mass Transfer, 125 (2018) 343–349.
[27] J. Shen, Z. Xing, X. Wang, Z. He, Analysis of a single-effect mechanical vapor compression desalination system using water injected twin screw compressors, Desalination, 333 (2014) 146–153.
[28] L. Gong, S. Shen, H. Liu, X. Mu, X. Chen, Three-dimensional heat transfer coefficient distributions in a large horizontal-tube falling film evaporator, Desalination, 357 (2015) 104–116.
[29] V.K. Patel, R.V. Rao, Design optimization of shell-and-tube heat exchanger using particle swarm optimization technique, Appl. Therm. Eng., 30 (2010) 1417–1425.
[30] B. Hu, D. Wu, R.Z. Wang, Water vapor compression and its various applications, Renewable Sustainable Energy Rev., 98 (2018) 92–107.
[31] C. Liu, M. Bi, Y. Zhou, G. Cui, A novel model for evaporator structural design in the multi-effect evaporation plant,

Appl. Therm. Eng., 176 (2020) 115351, doi: 10.1016/j.applthermaleng.2020.115351.
[32] P. Palenzuela, A.S. Hassan, G. Zaragoza, D.C. Alarcón-Padilla, Steady state model for multi-effect distillation case study: Plataforma Solar de Almería MED pilot plant, Desalination, 337 (2014) 31–42.
[33] H. El-Dessouky, I. Alatiqi, S. Bingulac, H. Ettouney, Steady-state analysis of the multiple effect evaporation desalination process, Chem. Eng. Technol., 21 (1998) 437–451.
[34] H. Yin, H. Wu, Y. Li, J. Quan, Performance analysis of the water-injected centrifugal vapor compressor, Energy, 200 (2020) 117538, doi: 10.1016/j.energy.2020.117538.
[35] A.M. El-Nashar, Economics of small solar-assisted multiple-effect stack distillation plants, Desalination, 130 (2000) 201–215.
[36] M. Papapetrou, A. Cipollina, U. La Commare, G. Micale, G. Zaragoza, G. Kosmadakis, Assessment of methodologies and data used to calculate desalination costs, Desalination, 419 (2017) 8–19.
[37] A. Piacentino, Application of advanced thermodynamics, thermoeconomics and exergy costing to a multiple effect distillation plant: in-depth analysis of cost formation process, Desalination, 371 (2015) 88–103.
[38] W. El-Mudir, M. El-Bousiffi, S. Al-Hengari, Performance evaluation of a small size TVC desalination plant, Desalination, 165 (2004) 269–279.
[39] Y.M. El-Sayed, Designing desalination systems for higher productivity, Desalination, 134 (2001) 129–158.
[40] Y. Wang, N. Lior, Thermoeconomic analysis of a low-temperature multi-effect thermal desalination system coupled with an absorption heat pump, Energy, 36 (2011) 3878–3887.
[41] B. Rahimi, Z. Marvi, A.A. Alamolhoda, M. Abbaspour, H.T. Chua, An industrial application of low-grade sensible waste heat driven seawater desalination: a case study, Desalination, 470 (2019) 114055, doi: 10.1016/j.desal.2019.06.021.
[42] M. Alsehli, M. Alzahrani, J.K. Choi, A novel design for solar integrated multi-effect distillation driven by sensible heat and alternate storage tanks, Desalination, 468 (2019) 114061, doi: 10.1016/j.desal.2019.07.001.